ACS Catalysis

pubs.acs.org/acscatalysis
Research Article

Electrocatalytic Hydrogenation of Glucose and Xylose on Electrochemically Roughened Metal Catalysts

Jay Pee Oña, Rose Marie Latonen, Narendra Kumar, Jan-Erik Eriksson, Ilari Angervo, and Henrik Grénman*

Cite This: ACS Catal. 2023, 13, 14300−14313
Read Online

ACCESS | Metrics & More | Article Recommendations | Supporting Information

ABSTRACT: Electrocatalytic hydrogenation (ECH) of glucose and xylose was studied on Ag, Au, Cu, Pt, and Zn polycrystalline metals. The metal catalysts were roughened electrochemically to expose more active sites. Estimates of surface roughness obtained from the determination of electrochemical surface areas (ECSA) were consistent with those obtained from physical measurements (i.e., confocal white light microscopy). The rough Cu catalyst gave the highest selectivity of 21.1% toward sorbitol production for a glucose conversion of 25.7% and the highest xylitol selectivity of 67.1% for a xylose conversion of 30.8%. Aside from hydrogenation products, significant amounts of 2-deoxyxylitol were formed over the Ag and Zn catalysts during xylose ECH. The results obtained demonstrate the dependence of ECH rate and product selectivity on the chemical properties of the metal catalysts. pH studies of ECH reactions show that appreciable yields of sorbitol and xylitol can be achieved at neutral pH (pH 7), with negligible formation of ketose side products. Furthermore, the Faradaic efficiency (FE) toward xylitol formation increased with more negative applied potentials and was highest at −1.0 V (vs RHE), while the maximum FE for sorbitol occurred at a less negative potential (−0.7 V). Therefore, the ECH rate depends not only on the amount of available chemisorbed hydrogen obtained from water splitting reactions but also on the reactivity of the substrate toward ECH. This work provides the basis for improving electrocatalytic systems for ECH of sugars and a step toward efficient valorization of these compounds from versatile biomass sources.

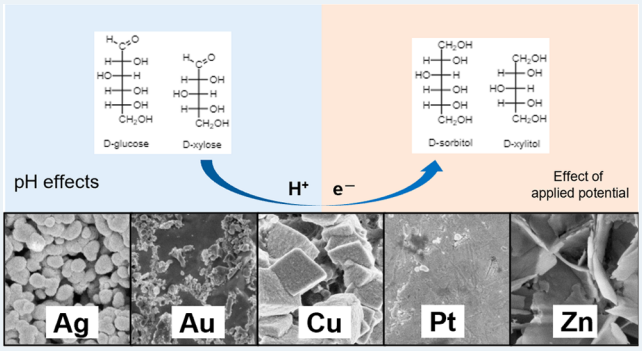

KEYWORDS: *electrocatalysis, surface roughness, xylose, glucose, hydrogenation, sorbitol, xylitol*

1. INTRODUCTION

The transition to sustainable production of fuels and chemicals, which would replace fossil-based alternatives, calls for environmentally friendly and cost-effective technologies for biomass valorization. Although biomass has the potential to satisfy a considerable part of the global demand for fuels and chemicals, its processing poses many technical challenges. To increase their energy density, it is beneficial for biomass compounds to have a high hydrogen content and low oxygen content.[1] However, conventional hydrotreatment and thermocatalytic hydrogenation at high H_2 pressures and temperatures are not easily applicable to biomass feedstocks due to the high water content and harmful side reactions that can deactivate the catalysts. Therefore, low-temperature hydrogenation processes in the aqueous phase need to be developed to upgrade biomass-derived compounds.

Electrocatalytic hydrogenation (ECH) has attracted attention in recent years as a feasible route for biomass upgrading due to its operability in aqueous feedstocks and mild reaction conditions. One advantage of ECH is that hydrogen can be derived directly from the electrolysis of water, thereby eliminating the need for a high-purity hydrogen supply. The energy supplied to power ECH can be derived from renewable electricity (e.g., solar, wind) which serves as the basis for energy storage in chemical bonds and decentralized production of fuels and value-added chemicals.[1] However, a better understanding of electrocatalytic systems is needed to make ECH technically feasible for widespread implementation.

Earlier studies on ECH of oxygenated compounds include phenol and benzaldehyde,[2−9] acids (e.g., levulinic, muconic, lactic acids),[10−14] furfural,[15−18] and sugars (e.g., glucose, glyceraldehyde).[19−25] Hydrogenation of the adsorbed substrate occurs via the addition of a chemisorbed hydrogen or through a proton-coupled electron transfer (PCET) in a sequential or concerted manner, as shown in Scheme 1.

Received: August 27, 2023
Revised: October 9, 2023
Accepted: October 11, 2023
Published: October 23, 2023

Scheme 1. Possible Reaction Pathways for the Electrochemical Hydrogenation Shown for a Sugar Molecule[a]

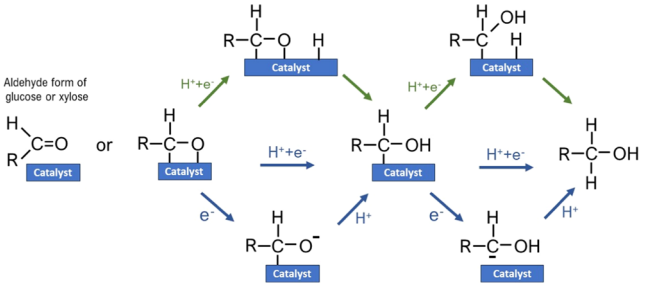

[a]Green arrows represent the mechanism that involves a chemisorbed hydrogen atom. Blue arrows indicate the simultaneous or sequential transfer of protons and electrons to the reacting species.

The chemisorbed hydrogen is formed over a metallic catalyst, *M* upon the application of a suitable electric potential (eq 1). Hydrogen evolution reaction (HER) then proceeds through the Tafel (eq 2) or Heyrovsky (eq 3) reactions:

$$H_2O + e^- + M \rightarrow MH + OH^- \text{ (Volmer reaction)} \quad (1)$$

$$2MH \rightleftharpoons 2M + H_2 \text{ (Tafel reaction)} \quad (2)$$

$$MH + H_2O + e^- \rightleftharpoons M + H_2 + OH^- \text{ (Heyrovsky reaction)} \quad (3)$$

The competing HER decreases the selectivity or Faradaic efficiency (FE) toward ECH, which depends on the surface coverage of adsorbed hydrogen and organic substrate.[26] The ECH rate of organic substrates has been observed to be influenced by the nature of the electrode material,[5,7,9,19,27] the catalyst surface,[3,4] electrolyte composition, and reaction conditions.[20,23−25,28,29] We have studied the ECH of glucose and xylose over carbon-supported gold catalysts[30,31] and observed the effects of the surface morphology of the catalyst, cluster size of the metal, and applied potential on the hydrogenation rate. Gold was chosen as a catalyst due to its selectivity toward sorbitol formation, based on the study by Kwon et al.[19] on electrocatalytic glucose hydrogenation. In the same study, other late transition metals (e.g., Fe, Co, Ni, Cu, Pd, Ag) were also observed to be selective toward sorbitol production. Due to the observed effects of catalyst surface morphology on the hydrogenation activity, it is worthwhile to explore and compare the activities of various metals (alongside Au), with modified surfaces to increase roughness, toward sugar ECH. Moreover, the effect of surface roughening on the catalytic activity and selectivity was studied for individual metal catalysts.

In this study, the ECH of glucose and xylose was studied on different metal catalysts (Ag, Au, Cu, Pt, and Zn). These metals exhibit different overpotentials for HER that is associated with their hydrogen binding energy.[32] The activity of these metals toward ECH would provide evidence of the reactivity of the sugars over the different metal surfaces. This could in turn help develop catalysts that are more selective for sugar ECH. Glucose and xylose were chosen as model compounds for the valorization of hemicellulose which can be extracted from wood biomass through hot water extraction.[33−35] Glucose and xylose monomers can be obtained from acid hydrolysis of hemicellulose in batch or continuous reactors.[36−38] The catalysts investigated were metal plate electrodes, which were electrochemically roughened to expose more active sites and to increase the rate of ECH of the sugars. The most active catalyst, namely, rough Cu, was studied in more detail at different experimental conditions (pH and electric potential) to determine ideal conditions for ECH.

2. EXPERIMENTAL SECTION

2.1. Materials. D-Glucose (BioUltra, ≥98 wt %) and D-xylose (BioUltra, ≥99% wt) reagents were obtained from Sigma-Aldrich. All other chemicals, Na_2SO_4, KCl, NaOH, H_2SO_4, and $HClO_4$, were of analytical grade and obtained from commercial sources. All solutions were prepared using deionized water (resistivity of 18 MΩ·cm).

2.2. Electrochemical Roughening of Metal Electrodes. Pure metal plates with geometric surface areas of 3−4 cm^2 were used in this research work. Prior to use, all of the metal electrodes were first polished with SiC paper and then with 0.3 μM alumina slurry. In between polishing steps, the electrodes were washed with deionized water and cleaned in an ultrasonic bath. The metal electrodes were then subjected to electrochemical roughening using a single-compartment electrochemical cell connected to a Gamry (ref 620) potentiostat. Except for Pt roughening, a Metrohm single-junction Ag/AgCl/3 M KCl reference electrode was used in all experiments. For all electrochemical procedures, the working solution was initially purged with N_2 gas for 15 min to remove dissolved oxygen, and the N_2 supply was kept above the surface of the liquid during each experiment. All electrochemical roughening procedures were carried out at room temperature (23 ± 2 °C).

2.2.1. Ag. The electrochemical roughening procedure for Ag was adopted from the work of Lian et al.[39] A silver metal plate (geometric area = 3 cm^2) was connected as the working electrode, and a glassy carbon (GC) rod was used as the counter electrode. The electrodes were immersed in 0.2 M KCl solution. Five (5) oxidation−reduction cycles (ORC) were made from −0.31 to +0.39 V at a scan rate of 5 mV s^{-1}. Afterward, the electrodes were washed with deionized water, and the working solution was replaced with 0.1 M Na_2SO_4. The potential was held at −0.31 V for 300 s, and the roughened Ag electrode was taken out of solution and rinsed thoroughly with deionized water.

2.2.2. Au. The gold catalyst was prepared following the electrochemical roughening procedure by Mie et al.[40] with modifications. A gold metal plate (4 cm^2) was immersed in 35 mM HCl and a potential of +1.21 V was applied for 30 min. The counter electrode used was a GC rod. The gold electrode was then thoroughly washed with deionized water. Afterward, the electrodes were immersed in 0.1 M Na_2SO_4 solution and the potential was swept linearly from 0.0 to −1.8 V at a scan rate of 5 mV s^{-1}. The roughened Au electrode was then washed thoroughly with deionized water.

2.2.3. Cu. The electrochemical roughening procedure for Cu was based on the work of Chen et al.[41] used to prepare stable Cu mesocrystals. A copper metal plate (4 cm^2) and a GC counter electrode were immersed in aqueous 0.1 M KCl. Five (5) ORCs were made from −0.32 to +1.18 V at a scan rate of 500 mV s^{-1}. During each cycle, the potential was held at the positive limit for 10 s and at the negative limit for 5 s. The Cu electrode was then washed thoroughly with deionized water. Afterward, the electrodes were immersed in 0.1 M Na_2SO_4 solution, and a potential of −1.3 V was applied to the Cu

https://doi.org/10.1021/acscatal.3c04043
ACS Catal. 2023, 13, 14300−14313

electrode for 3600 s. The roughened Cu electrode was then taken out of solution and washed with deionized water.

2.2.4. Pt. A three-electrode system was constructed using a platinum plate (4 cm^2) working electrode, a coiled platinum wire as counter electrode, and an Ag/Ag_2SO_4 pseudoreference electrode. The Ag/Ag_2SO_4 pseudoreference electrode was employed to prevent chloride contamination from an Ag/AgCl/3 M KCl reference electrode that could interfere with oxide formation. The potential difference between the Ag/Ag_2SO_4 pseudoreference electrode and a commercial Ag/AgCl/3 M KCl reference electrode was +0.28 V. The electrochemical roughening of the Pt plate electrode was carried out by running 200 ORCs between −0.4 and +2.4 V vs Ag/Ag_2SO_4 in 0.5 M H_2SO_4 at a scan rate of 100 mV s^{-1}. The potential range was based on the roughening procedure used by Weremfo et al.[42] for a Pt electrode. At the end of the potential cycling, the potential was maintained at −0.4 V for 30 min to reduce any surface oxide produced. Thereafter, the roughened Pt electrode was taken out of the working solution and washed thoroughly with deionized water.

2.2.5. Zn. The electrochemical roughening procedure for Zn used by Gu et al.[43] was employed to prepare the Zn catalyst. A zinc plate electrode was connected as a working electrode, and a GC rod was used as counter electrode. The electrodes were immersed in an aqueous 0.5 M $NaClO_4$ solution. Forty (40) ORCs were applied on the Zn electrode between −1.56 and −0.66 V at a rate of 50 mV s^{-1}. At the end of the ORCs, the potential was maintained at −1.56 V for 300 s to reduce the zinc oxide on the surface completely. Thereafter, the roughened Zn electrode was removed from the solution and washed with deionized water.

2.3. Characterization of the Textural Properties of Roughened Metal Catalysts. The surface morphologies of the roughened metal catalysts were studied by using scanning electron microscopy (SEM). The instrument used (Leo Gemini 1530) is equipped with a Thermo Scientific UltraDry Silicon Drift Detector. Energy-dispersive X-ray analysis (EDXA) was used to determine the chemical composition of the metal surfaces. Confocal white light microscopy (Nano-Focus μSurf) was used to take three-dimensional (3D) images of the roughened metal catalysts and to provide a quantitative estimate of the surface roughness of each metal electrode. The structural analysis and phase purity of the most active catalyst were carried out by X-ray powder diffraction using a diffractometer (PANalytical Empyrean) with five-axis goniometer. The supplied X-ray radiation (Empyrean Cu LFF) was filtered to include only Cu $K_{\alpha 1}$ and Cu $K_{\alpha 2}$ components. The results were analyzed using MAUD (Material Analysis Using Diffraction) program.

2.4. Electrochemical Measurements. Electrochemical characterizations were carried out by using cyclic voltammetry (CV) and linear sweep voltammetry (LSV). The measurements were conducted in an H-shaped electrochemical cell divided by a Nafion 117 membrane (Ion Power, Inc.). The cleaning procedure for the glass H-cell and Nafion membrane preparation can be found in our earlier studies.[30,31] The first chamber of the H-cell held the rough metal working electrode and the reference electrode (Ag/AgCl/3 M KCl, Thermo Scientific Orion 900100) immersed in 30 mL of the working solution (aqueous 0.1 M glucose or xylose with 0.1 M Na_2SO_4) while the second chamber contained the counter electrode in 30 mL of the supporting electrolyte solution (0.1 M Na_2SO_4). The counter electrode was constructed by attaching an activated carbon cloth (0.60 mm thickness, Kynol) to a carbon rod (99.999% carbon, Strem Chemicals, Inc.) using carbon glue (Electrodag PF-407C). The electric potential was supplied by a Gamry (Reference 620) potentiostat at room temperature (23 ± 2 °C). The applied potentials during electrochemical characterization and catalytic tests were converted from the Ag/AgCl to the RHE scale using the equation: $E(\mathrm{RHE}) = E(\mathrm{Ag/AgCl}) + E^{\circ}(\mathrm{Ag/AgCl}) + 0.059\mathrm{pH}$, where $E^{\circ}(\mathrm{Ag/AgCl})$ has the value of 0.197 V (potential of Ag/AgCl/3 M KCl versus the normal hydrogen electrode) and the pH corresponds to the pH of the reaction solution. In all experiments, the working solution was purged with N_2 gas prior to measurement and the N_2 gas supply was maintained on the surface of the liquid throughout the measurement.

The electrochemically active surface areas (ECSA) of the roughened metal electrodes were estimated by measuring their double-layer capacitance with a cyclic voltammetric procedure as described by McCrory et al.[44] The CV measurements were carried out in an H-shaped electrochemical cell divided by a Nafion 117 membrane. One compartment contained the roughened metal as a working electrode and reference electrode immersed in 25 mL of 1 M NaOH. The other compartment contained the counter electrode immersed in 25 mL of 1 M NaOH solution. The potential range of the CV was 0.1 V and was centered at the open circuit potential (OCP) of the system. At this range, all of the currents generated are associated with non-Faradaic processes. During the CV, the potential was swept from the more positive potential toward the more negative potential and back for three cycles. The working electrode was held at each potential vertex for 10 s before the next sweep. CV was carried out using 6 different scan rates: 1, 5, 7.5, 10, 20, and 50 mV s^{-1}, and three cycles were recorded for each scan rate.

2.5. Electrocatalytic Hydrogenation of Glucose and Xylose. The activity of the roughened metal catalysts toward glucose and xylose ECH was tested by constant-potential electrolysis using the H-shaped electrochemical cell configuration described in 2.4. The designated potentials were applied to each of the working electrodes for 6 h in a solution of 0.1 M glucose or 0.1 M xylose with 0.1 M Na_2SO_4 supporting electrolyte at room temperature (23 ± 2 °C). During the reaction, the solution was magnetically stirred at approximately 500 rpm. Samples were collected from the reaction solution during electrolysis and analyzed.

Optimization experiments for reaction conditions (pH, applied potential) were carried out in a single-compartment electrolytic cell with the temperature maintained at 25 °C by using a thermal bath. The designated pH was maintained by the addition of 1 M NaOH or 1 M H_2SO_4 using an automatic titrator (Metrohm 799 GPT Titrino) equipped with a pH sensor. The reaction solution was stirred during electrolysis by using a magnetic stirrer set at approximately 500 rpm. The reaction products were analyzed using HPLC with a refractive index detector. Samples collected were immediately neutralized to pH 7 using dilute NaOH or H_2SO_4 solution. The HPLC column used was an Aminex HPX-87C that was maintained at 50 °C and the eluent was 1.2 mM $CaSO_4$ solution at a flow rate of 0.3 mL min^{-1}.

3. RESULTS AND DISCUSSION

3.1. Surface Characteristics of Roughened Metal Electrodes. *3.1.1. Ag.* The surface of the Ag electrode was roughened by successive ORCs in 0.2 M KCl and subsequent

https://doi.org/10.1021/acscatal.3c04043
ACS Catal. 2023, 13, 14300−14313

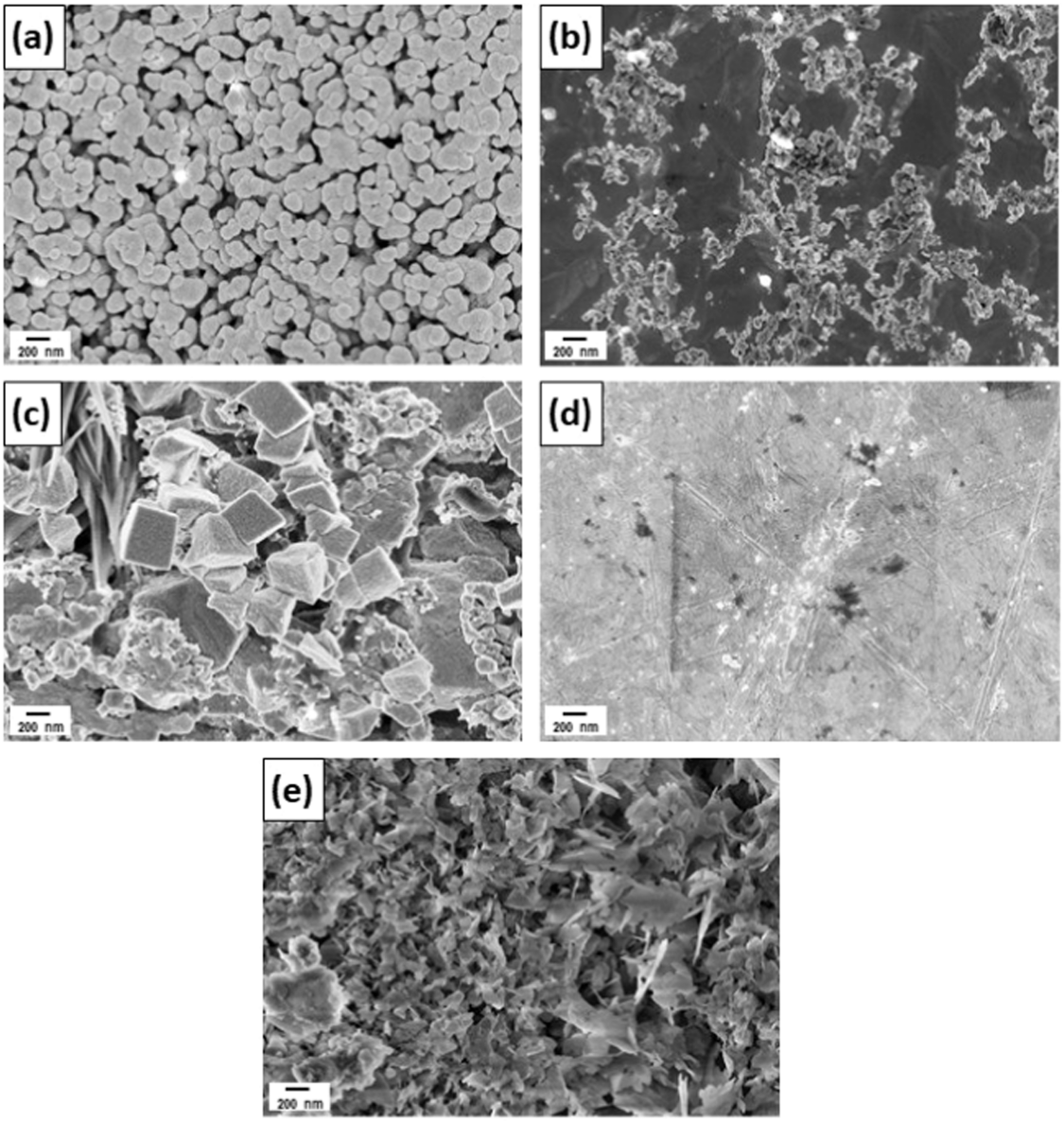

Figure 1. Scanning electron micrographs of electrochemically roughened Ag (a), Au (b), Cu (c), Pt (d), and Zn (e).

reduction in 0.1 M Na_2SO_4. As seen from the SEM image (Figure 1a), the surface of the roughened Ag became nanoporous with ligaments 100−300 nm in size compared to the unroughened Ag surface (Figure S1a). The cyclic voltammogram recorded in 0.2 M KCl (Figure S2) during the roughening procedure showed a main oxidation peak at ca. + 0.35 V and a reduction peak at ca. −0.30 V. The anodic peak is attributed to the oxidation of Ag^0 to Ag^+ and the simultaneous formation of a Ag−Cl complex. The formation of the Ag−Cl complex slowed down the diffusion and subsequent reduction of Ag^+ ions, which helped to form small Ag nanoparticles.[39] The resulting surface had a Ag purity of 98% wt as obtained from EDXA (Figure S4a and Table S1).

3.1.2. Au. The Au electrode was oxidized by applying a constant potential of +1.21 V in 36 mM HCl and was subsequently reduced in 0.1 M Na_2SO_4 to facilitate the removal of chloride ions. During the anodization, Cl^- ions aid in the dissolution of gold, which is followed by disproportionation of Au−Cl complexes and deposition as nanoporous gold.[40] The procedure resulted in the formation of a network of irregularly shaped gold nanoparticles (Figure 1b) compared to the Au surface before electrochemical roughening (Figure S1b). A closer look at the surface shows gold nanoparticles with sizes of 50−150 nm (Figure S3) with high Au purity of 97% (Table S1).

3.1.3. Cu. Electrochemical roughening of a polished Cu plate was accomplished by running 5 ORCs between −0.32 and +1.18 V in 0.1 M KCl and subsequent reduction by applying −1.3 V in 0.1 M Na_2SO_4. This procedure resulted in the formation of Cu mesocrystals in the form of cuboids 300−500 nm in size (Figure 1c) that were absent in the unroughened Cu surface (Figure S1c). The formation of Cu mesocrystals is assumed to proceed via the dissolution of the $CuCl_2$ layer formed from the oxidation−reduction cycles during the reduction step and further redeposition of the Cu atoms on the surface of the metal.[41] Analysis of the roughened Cu surface by EDXA showed high Cu purity (95 wt %) with no Cl or $CuCl_2$ contaminants (Figure S4c).

3.1.4. Pt. Electrochemically roughening of Pt was carried out by subjecting the plate electrode to 200 ORCs between −0.4

https://doi.org/10.1021/acscatal.3c04043
ACS Catal. 2023, 13, 14300−14313

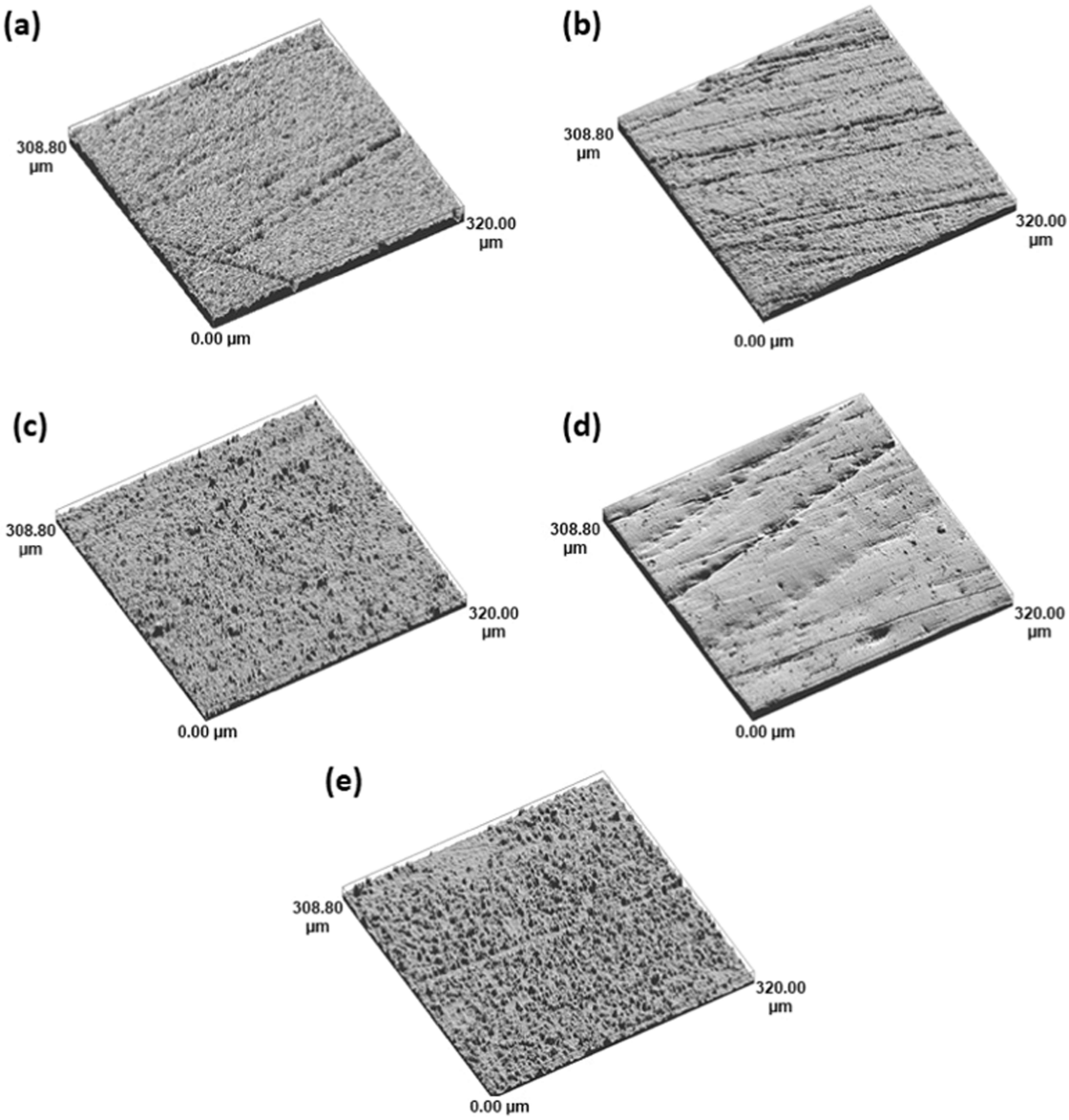

Figure 2. Confocal white light micrographs of Ag (a), Au (b), Cu (c), Pt (d), and Zn (e) after electrochemical roughening. Images were obtained by using a 50× magnification lens and a cutoff wavelength of 80 μm.

and +2.4 V vs Ag/Ag_2SO_4 in 0.5 M H_2SO_4 and subsequent reduction in the same solution at −0.4 V for 30 min. The repeated ORCs facilitated the formation of surface oxides, which would then introduce irregularities on the Pt surface upon reduction.[42] Figure 1d shows the electrochemically roughened Pt surface. Compared to the unroughened Pt electrode (Figure S1d), there was only a slight change in the surface morphology of the roughened electrode. Using repeated square wave cycles in the same potential range, a higher degree of roughness was previously obtained for a Pt electrode.[42] EDXA of the roughened Pt metal showed 100% (wt) purity (Figure S4d).

3.1.5. Zn. A Zn plate electrode was roughened electrochemically by running 5 ORCs between −1.56 and −0.66 V and subsequent reduction at −1.56 V for 300 s in 0.5 M $NaClO_4$ solution. The increase in anodic current in the cyclic voltammogram (Figure S5) is associated with the formation of zinc oxide on the surface of the electrode.[43] In the reverse scan, a cathodic peak at ca. −1.2 V can be observed, which corresponds to the reduction of zinc oxide. Analysis of the roughened Zn showed 92% purity with O, S, and Cu contaminants. The SEM image of the roughened Zn electrode (Figure 1e) showed flake structures with sizes from 200 to 750 nm (Figure S6), which were not present in the unroughened Zn electrode (Figure S1e).

XRD analyses of the roughened metal plates showed texturized diffraction patterns that match a face-centered cubic crystal for the Ag, Au, Cu, and Pt catalysts (Figure S8a–d). The Zn plate, on the other hand, showed mixed diffraction patterns that can be assigned to Zn, ZnO, and $Zn(OH)_2$ (Figure S8e). The diffraction peaks correspond to the hexagonal structure of Zn and wurtzite ZnO. The diffraction data are summarized in Table S2 in the Supporting Information.

Confocal white light microscopy was used to characterize the surface of the electrochemically roughened metal electrodes and to provide a physical measure of the surface roughness. The 3D micrographs of the rough metals are shown in Figure

https://doi.org/10.1021/acscatal.3c04043
ACS Catal. 2023, 13, 14300−14313

2. The images shown were determined from photorealistic shading and not from actual photographs. The parameter used to describe the surface roughness is the arithmetic average height (*Sa*), which is defined as the average absolute deviation from the mean line drawn over the sampling length.[45] A higher *Sa* value indicates a higher degree of roughness. *Sa* values determined for the roughened metal electrodes are listed in Table 1. The highest *Sa* was measured for Zn (0.77 μm)

Table 1. Experimental ECSA, RF, and *Sa* Values Obtained for the Different Roughened Metals

roughened metal	electrochemically active surface area (ECSA, cm^2)	roughness factor (RF)	arithmetic average height (*Sa*, μm) (confocal white light microscopy)
Ag	8.5 ± 1.0	3.1 ± 0.4	0.19 ± 0.05
Au	6.1 ± 1.4	1.5 ± 0.4	0.17 ± 0.05
Cu	88.9 ± 1.9	22.2 ± 0.5	0.31 ± 0.01
Pt	6.0 ± 0.5	1.5 ± 0.1	0.06 ± 0.01
Zn	182.5 ± 22.6	45.6 ± 5.7	0.77 ± 0.36

(Figure 2e). On the other hand, the lowest degree of roughness was observed with the roughened Pt metal (*Sa* = 0.056 μm). As can be observed in the SEM (Figure 1d) and confocal white light (Figure 2d) micrographs, Pt had a smoother surface than the other roughened metals.

The experimentally obtained ECSA (see Section S2.1 in the Supporting Information) was used to determine the roughness factor (RF) of each of the roughened metals calculated by dividing the ECSA by the geometric area of the electrode. The ECSA and RF values for the roughened metals are listed in Table 1. Due to inaccuracies associated with the method for determining ECSA, it is estimated that the values are accurate within an order of magnitude.[44] However, this method was used in the present study to provide an estimate of roughness using a uniform method for determining the ECSA. Furthermore, the experimentally obtained RF values were used as an approximate guide in comparing surface roughness.

The RF values obtained from ECSA measurements and *Sa* values from confocal white light microscopic analysis were plotted together in Figure 3. As seen from the plot, the *Sa* values were consistent with the trend for the RF values, which would then provide a good basis for comparing the specific activities of the metal catalysts toward sugar ECH.

3.2. Glucose and Xylose ECH over Rough Metal Catalysts. Figure 4 shows the linear sweep voltammograms of the roughened metal electrodes recorded in the pure electrolyte and in the presence of 0.1 M glucose (Figure 4a,b) and 0.1 M xylose (Figure 4c,d). The current density was expressed as the current normalized to the ECSA of each of the rough metal electrodes. The dashed lines represent the voltammograms recorded in the pure electrolyte (0.1 M Na_2SO_4), where the cathodic currents are associated with the reduction of water to H_2 (HER). HER is indicated by the gradual increase in cathodic current and occurs starting at ca. −0.7 V for Ag and Au, −0.8 V for Zn, and ca. −0.6 V for Cu. The onset of HER occurs earlier for Pt at ca. −0.4 V. The current densities for the rough Cu and Zn metals (Figure 4b,d) were significantly lower than for the other metals owing to their much higher ECSA. Furthermore, a cathodic peak is visible with the voltammogram of Zn in the pure electrolyte at ca. −0.7 V which may be due to the reduction of zinc oxide on the surface of the metal. Tafel plots derived from LSV curves in 0.1 M Na_2SO_4 are shown in Figure S10 and the corresponding Tafel slopes are listed in Table S3. The magnitude of the Tafel slope increased according to the following trend: Pt < Ag < Cu < Zn < Au. A smaller Tafel slope often indicates faster HER kinetics,[46] and experimental results show higher HER activity over Pt than on the other metals. Aside from the intrinsic catalytic activity, higher ECSA also contributes to higher HER activity,[44] which would explain the lower Tafel slope of Zn (285 mV dec^{-1}) than Au (295 mV dec^{-1}). A theoretical Tafel slope value of 120 mV dec^{-1} characterizes HER mechanisms limited by the Volmer or Hevrovsky steps (eqs 1 and 3).[47] Deviations of experimental slopes from this theoretical value could arise from the near-neutral pH (~6.8) of the electrolyte solution, wherein the HER activity is lower than in acidic conditions.[48]

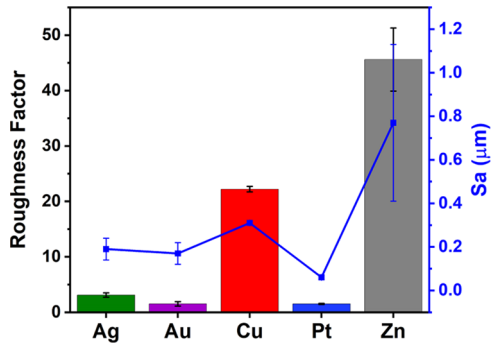

Figure 3. Plot of the roughness factor (RF, colored bars) values obtained from ECSA measurements against roughness estimates (arithmetic average height, *Sa*, connected blue squares) derived from confocal white light microscopy for the roughened metal catalysts.

In the presence of glucose, the cathodic currents were observed to be higher compared to those from HER for Ag, Au (Figure 4a), and Cu (Figure 4b), which indicates that the reduction of glucose is easier than water reduction on these metals. Using voltammetry with online product analysis, Kwon et al. showed that sorbitol is formed over Ag, Au, and Cu starting from −0.9, −0.7, and −0.75 V (vs RHE).[19] This indicates that glucose ECH occurs concurrently with HER over Ag, Au, and Cu since hydrogen gas evolution was also visible during LSV in the sugar solutions. In the xylose solution, the cathodic current was also higher than in the pure electrolyte for the Ag electrode, while there was no observable change in current density for Au (Figure 4c). For the Cu catalyst, a cathodic peak was visible at ca. −0.7 V in xylose solution (Figure 4d), which may be due to the reduction of xylose, and current density was lower compared to that of HER starting from −0.8 V. Lower cathodic current was also observed for the rough Zn electrode in 0.1 M glucose (Figure 4b) and in 0.1 M xylose (Figure 4d) starting from ca. −0.8 V compared to HER conditions. The decrease in current density may be due to the adsorption of sugar molecules on the metal surface, which then suppressed the HER in both Cu and Zn electrodes. In contrast, for the Pt metal, the cathodic current increased from a more positive potential in the presence of glucose (Figure 4a) or xylose (Figure 4c) (both at ca. −0.2 V) than in the pure electrolyte (ca. −0.4 V). This would indicate that surface reactions involving glucose or xylose occur before the onset of the HER over the Pt catalyst.

Constant-potential electrolyses were conducted in an unbuffered solution of 0.1 M glucose or xylose in 0.1 M Na_2SO_4 to determine the hydrogenation activity of each metal

https://doi.org/10.1021/acscatal.3c04043
ACS Catal. 2023, 13, 14300−14313

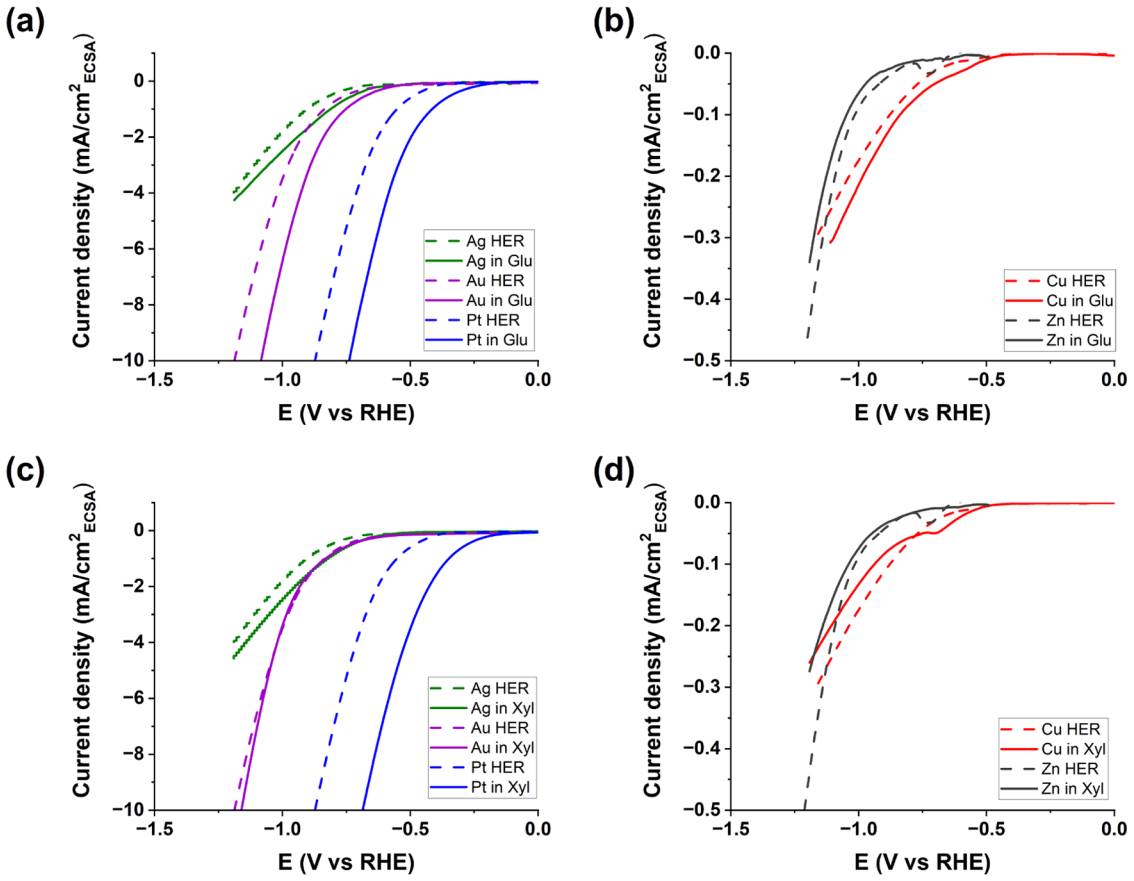

Figure 4. Linear sweep voltammograms of the rough metal electrodes in 0.1 M glucose (a, b) and in 0.1 M xylose (c, d) with 0.1 M Na_2SO_4 supporting electrolyte. Dashed lines represent the voltammograms recorded in the pure electrolyte. The scan rate used was 5 mV s^{-1}.

Table 2. Constant-Potential Electrolysis Data from Glucose and Xylose ECH over the Rough Metal Catalysts

metal catalyst	applied potential (V vs RHE)	glucose conversion (%)	sorbitol FE (%)	total charge (C)	carbon balance (%)
		Glucose ECH			
Ag	−1.12	15.9 ± 2.2	0.5 ± 0.1	667 ± 49	95.4 ± 1.1
Au	−1.09	11.5 ± 2.0	0.4 ± 0.1	780 ± 27	97.8 ± 2.4
Cu	−0.99	25.7 ± 1.3	2.4 ± 1.1	1117 ± 60	95.4 ± 2.9
Pt	−0.79	16.7 ± 1.0		277 ± 10	95.3 ± 1.4
Zn	−1.19	4.8 ± 0.5	1.1 ± 0.5	247 ± 2	84.5 ± 4.4
metal catalyst	applied potential (V vs RHE)	xylose conversion (%)	xylitol FE (%)	total charge (C)	carbon balance (%)
		Xylose ECH			
Ag	−1.12	18.3 ± 2.5	4.5 ± 0.2	577 ± 61	97.6 ± 1.5
Au	−1.09	8.7 ± 3.0	0.3 ± 0.2	630 ± 67	68.2 ± 2.5
Cu	−0.99	30.8 ± 4.8	9.8 ± 3.9	1087 ± 13	90.6 ± 1.2
Pt	−0.79	8.3 ± 2.4	0.4 ± 0.1	260 ± 21	78.3 ± 5.0
Zn	−1.19	16.1 ± 5.4	2.8 ± 1.2	391 ± 20	95.7 ± 2.8

catalyst. The applied potentials used during electrolyses are listed in Table 2 and were determined from the LSV experiments in a pure 0.1 M Na_2SO_4 solution (Figure S9), where the potential on each metal catalyst corresponds to a current density of 10 mA $cm_{geometric}^{-2}$. These applied potentials would also correspond to the Tafel constants when defined as the overpotential at 10 mA $cm_{geometric}^{-2}$ current density ($\eta_{j=10}$) as shown in the Tafel plots for the metals (see Figure S10). Also shown in Table 2 are the calculated Faradaic efficiencies toward sorbitol or xylitol formation using the following equation:

$$\text{FE}\ (\%) = \frac{\text{mol of hydrogenation product}}{\text{total charge passed}\ (C)/(F{\cdot}2)} \times 100 \quad (4)$$

where the total charge is expressed in coulombs (C) and F represents the Faraday's constant (96,485 C mol^{-1}) and the theoretical number of exchanged electrons is two (2) electrons. The total charge is determined from the current vs time plot obtained from the chronoamperometric experiments in glucose and xylose solutions (shown in Figure S11).

Figure 5 shows the conversion of glucose (Figure 5a) and xylose (Figure 5c) over the different metal catalysts during the 6 h electrolysis experiments and the selectivity to various products recorded after the reaction period (Figure 5b,d). The

https://doi.org/10.1021/acscatal.3c04043
ACS Catal. 2023, 13, 14300−14313

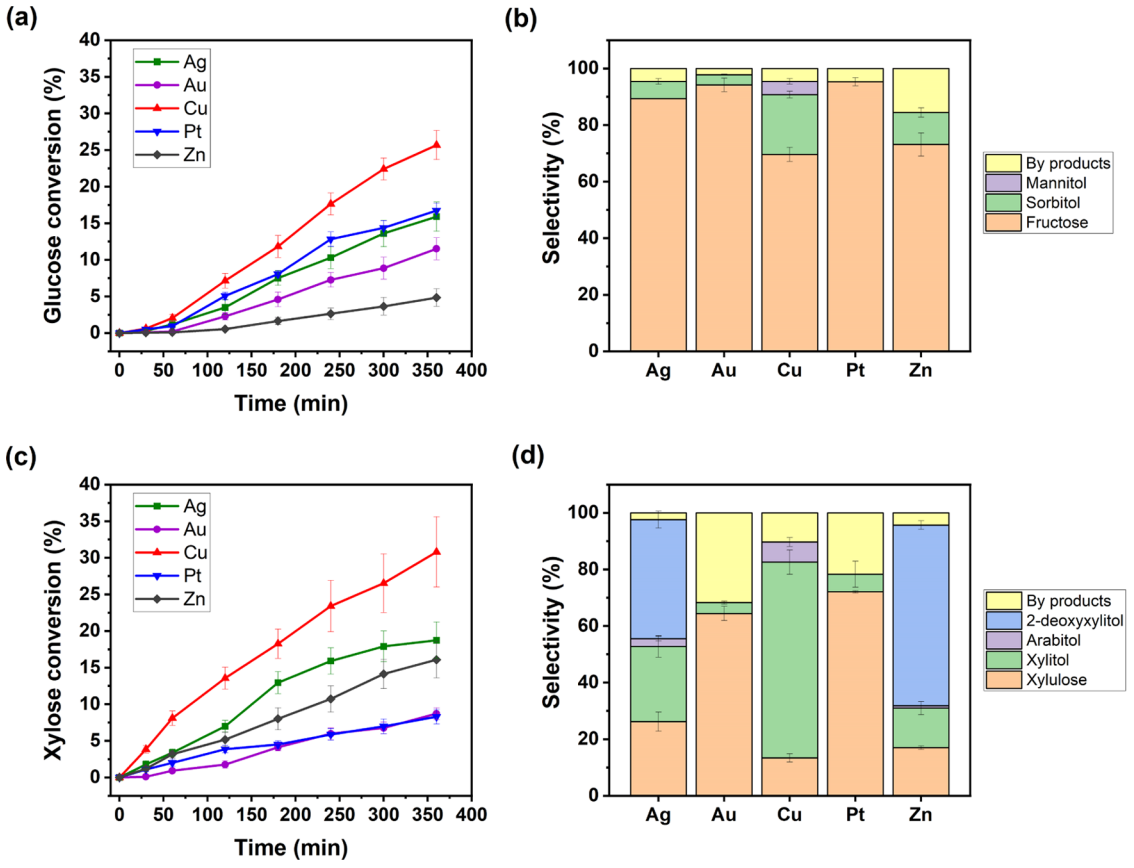

Figure 5. Relative conversions (%) of glucose (a) and xylose (c) during a 6 h constant-potential electrolysis carried out in 0.1 M glucose or xylose in 0.1 M Na_2SO_4 supporting electrolyte. The selectivity (%) to the different reaction products from glucose (b) and xylose (d) ECH was determined after the 6 h reaction period. ECH reactions were done at room temperature and pressure with a stirring speed of 500 rpm.

HPLC chromatograms of the reaction products from glucose and xylose ECH are provided in Figure S12. The carbon balance listed in Table 2 was calculated from the sum of the selectivity of each known reaction product (Table S4). Deficiencies in carbon balance arise from limitations in product identification from HPLC analysis. For the glucose ECH, the conversion of glucose observed on all metal catalysts was mostly due to the isomerization into fructose, as can be seen in Figure 5b. Sorbitol formation was observed over the Ag, Au, Cu, and Zn catalysts, with the highest selectivity of 21.1% recorded for Cu for a conversion of 25.7% (Figure 5a). Aside from sorbitol, mannitol formation was also observed over the rough Cu catalyst with a corresponding selectivity of 4.7%. Mannitol is assumed to be formed from fructose, as mannose was not detected at any point during the reaction. This is supported by the study conducted by Owobi-Andely et al.,[29] wherein fructose was hydrogenated with a similar ratio into sorbitol (40%) and mannitol (60%). On the Ag and Au catalysts, the glucose conversion and sorbitol selectivity were slightly higher for Ag (6.1% selectivity for 15.9% conversion) than Au (3.6% selectivity for 11.5% conversion). The absence of mannitol in the reaction product on either Ag or Au suggests that sorbitol formation arises from glucose. Although the glucose conversion over Zn was the lowest among the studied catalysts, the selectivity toward sorbitol formation over Zn (11.3%) was higher than either Ag or Au. The lower glucose conversion on Zn is due to the suppression of HER in the presence of glucose, as evident from the linear sweep voltammetry experiments (Figure 4b). HER suppression would result in less production of hydroxide ions that convert glucose into fructose, as will be described later. Furthermore, unidentified products were formed over Zn which accounted for the deficiency in carbon balance (84.5%, Table 2). We suspect that these are deoxygenated products as observed in the work by Kwon et al.,[19] but the concentrations are quite low to be confirmed by NMR spectroscopy. In contrast, fructose was the major product over Pt, the most active catalyst toward the HER, with a selectivity of 95.4%, without observable formation of hydrogenation products. Comparing the product distribution after 3 and 6 h of electrolysis (Figure S13a), the relative concentration of fructose increased at the end of the 6 h electrolysis period over all of the metal catalysts except for Cu, without any observable formation of mannitol. For the rough Cu catalyst, the selectivity to fructose remained roughly the same between 3 and 6 h of reaction, while the selectivity to mannitol increased from 1.1 to 4.7%, which further supports the assumption that fructose is the precursor for mannitol formation. In terms of current efficiency, the highest FE toward sorbitol formation was recorded for Cu (2.4%), followed by Zn (1.1%), Ag (0.5%), and Au (0.4%) (Table 2). The mannitol FE over Cu was 0.5%, which was lower than that for sorbitol. The observed FEs for the sugar alcohols were generally low, which indicates that the charge supplied during glucose ECH proceeded mostly toward the HER.

For the xylose ECH, xylitol was formed over all of the studied catalysts with the highest selectivity of 67.1% observed for the rough Cu catalyst for a conversion of 30.8% (Figure 5c,d). Higher xylose conversion and xylitol selectivity were

https://doi.org/10.1021/acscatal.3c04043
ACS Catal. 2023, 13, 14300−14313

observed for the rough Ag catalyst (26.6% selectivity for 18.7% conversion) than Zn (14.0% selectivity for 16.1% conversion). Relatively lower xylitol selectivity was observed for the Au and Pt catalysts, with 3.8 and 6.2%, respectively. A similar extent of xylose conversion was observed for Au (8.7%) and Pt (8.3%), where the conversion was due to the formation of xylulose and other byproducts on both metals (Figure 5d). Unidentified products over Au and Pt resulted in deficiencies in carbon balance (68.2 and 78.3%, respectively). Arabitol was formed only on Cu, Ag, and Zn, with selectivity of 6.9, 2.7, and 0.8%, respectively. Analogous to glucose ECH, arabitol is assumed to be formed from the ketose isomer of xylose, xylulose. Looking at the product distribution on each of the metal catalysts between 3 and 6 h of reaction, there was a general decrease in selectivity toward xylulose (Figure S13b). This indicates that xylulose was consumed alongside xylose during the progress of electrolyses. The highest xylitol FE was also observed for the rough Cu catalyst (9.8%) followed by Ag, Zn, Pt, and Au (Table 2). On the other hand, the FEs for arabitol formation on Cu, Ag, and Zn were 1.0, 0.2, and 0.2%, respectively. Similar to the glucose ECH, HER was the major competing reaction during the ECH of xylose. However, the FEs toward the formation of hydrogenation products were higher for xylose ECH than those for glucose ECH (Table 2). This would indicate higher reactivity of xylose than glucose toward ECH over the prepared (electro)catalysts under the same reaction conditions.

Aside from hydrogenation products, the formation of deoxygenated products was detected by NMR spectroscopy from the ECH of xylose over the roughened Ag and Zn catalysts. The NMR spectra show the presence of deoxyxylitol in the ECH products over Ag and Zn catalysts after 6 h of electrolysis (Figure S14). Analysis using $^{1}H-^{1}H$ correlated spectroscopy (COSY) indicates that the product formed was 2-deoxyxylitol (Figure S15). The formation of deoxy sugars was observed in earlier studies on glucose ECH by Nobe et al.[24] over Raney Ni and by Kwon et al.[19] over Zn metal, where 2-deoxysorbitol was identified as the product. Nobe et al. suggested that fructose, formed from the base-catalyzed isomerization of glucose, was reduced over Raney Ni producing 2-deoxysorbitol. On the other hand, Kwon et al. suggested that glucose itself could be the precursor to 2-deoxysorbitol, as the C−O bond preferentially breaks in the C−OH group adjacent to the carbonyl group in the reduction of 2-carbon oxygenates,[49] as well as for other monosaccharides.[25]

To investigate the effect of surface roughening with the present rough metal catalysts, we tested the ECH activities on smooth metal catalysts and compared them with those of the roughened metals. Figure S16 shows the catalytic values for xylose ECH from the three most active catalysts, Ag, Cu, and Zn. Xylose ECH was carried out at −1.26, −1.09, and −1.19 V (vs RHE) over the smooth Ag, Cu, and Zn, respectively, to match the potentials at which the current density was 10 mA cm^{-2}. The positive effect of roughening on the FE toward xylitol formation can be observed with all of the metals, with an increase in FE values by a factor of approximately 12, 3, and 7 for Ag, Cu, and Zn, respectively (Figure S16b). The overall xylose conversion increased with higher surface roughness for Ag and Cu (Figure S16a) but not for Zn. This is due to the higher concentration of xylulose in the product solution over the smooth Zn than the rough metal formed from the isomerization of xylose.

The shape of the polycrystalline metal catalyst also influenced the ECH rate, as observed for the Ag metal in planar and rod (cylindrical form). As shown in Figure S17, the sugar conversion was higher for the planar Ag than for a rod after a fixed electrolysis period. However, the product distribution was similar for both planar and rod geometry. This relates to the surface contact between the catalyst and reacting species, which is important to consider in the design of efficient catalysts for ECH reactions.

In order to estimate the specific activity of the metal catalysts toward glucose and xylose ECH, the amount of sorbitol and xylitol produced over each metal was normalized to its ECSA. From the ECSA-normalized yields for sorbitol and xylitol (Figure S18) over the metal catalysts, the specific activity toward glucose ECH followed the trend Ag > Au > Cu > Zn > (Pt), while the trend for xylose ECH was Ag > Cu > Au > Pt > Zn. In terms of ECH of carbonyl functionality, Roylance et al. observed a higher activity of a Ag catalyst (prepared by sputtering or galvanic displacement) compared to a metallic Cu catalyst toward ECH of 5-hydroxymethylfurfural (HMF).[16] In the study by Kwon et al. on the ECH of glucose,[19] Au and Cu showed comparable yields of sorbitol but at different applied potentials, namely, −1.05 V (vs RHE) for Au and −1.3 V (vs RHE) for Cu. Pt metal was also found to be inactive toward glucose ECH, possibly due to the faster kinetics toward HER than ECH. The same study showed that sorbitol was formed over a Zn catalyst with lower yield than Au or Cu.[19] The trends observed for specific activities in this study, however, rely only on the electrochemically active sites, which may not have equal reactivity from one metal to another. Therefore, a deeper investigation of the fundamental properties of the catalyst and its interaction with the sugar substrate is necessary. For instance, Lopez-Ruiz et al. have demonstrated the correlation between the rates of ECH of the carbonyl group and the binding energy between the aldehyde molecule and the metal.[9] Furthermore, the ECSA and hence the roughness factor were observed to increase for the Ag, Cu, and Zn catalysts over the course of the ECH reactions (see Table S5), while those for Au and Pt remained constant. This indicates that the Ag, Cu, and Zn catalysts undergo surface structural changes during ECH reactions, which makes the assignment of ECSA to obtain normalized activities more difficult for these metals. SEM analysis of the spent Ag and Cu catalysts confirmed these modifications in the surface morphology (Figure S19). For the spent Ag, the spaces between the ligaments became larger, giving higher porosity to the bulk structure (Figure S19a). For the spent Cu catalyst, smaller nanostructures developed over the initially formed cuboid structures (Figure S19b), similar to that observed by Chen et al. during CO_2 electroreduction over Cu mesocrystals.[41] The apparent increase in porosities may have contributed to the increase in double-layer capacitance in the spent Ag, Cu, and Zn and therefore the resulting ECSA. In contrast, the *Sa* values measured for the spent Ag, Cu, and Zn catalysts by confocal microscopy were lower than those obtained before the catalytic tests. This is possibly due to the increased surface homogeneity in the spent catalysts. Meanwhile, the *Sa* for Au remained the same and slightly decreased for spent Pt. The overall trend in *Sa* values, however, was the same as for the freshly prepared catalysts.

From the catalytic results, it was demonstrated that a Cu catalyst with suitable roughness would be active toward sugar hydrogenation, especially for xylose ECH. Bulk Cu metal was

https://doi.org/10.1021/acscatal.3c04043
ACS Catal. 2023, 13, 14300−14313

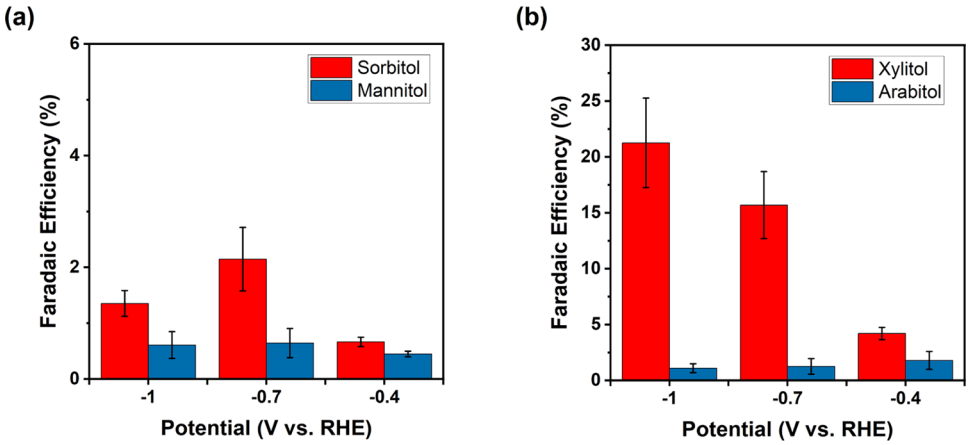

Figure 6. Faradaic efficiencies of glucose (a) and xylose (b) ECH products over a rough Cu catalyst. Constant-potential electrolyses were carried out in 0.1 M glucose or xylose with 0.1 M Na_2SO_4. The pH of the reaction solution was maintained at pH 7 at 25 °C with a stirring speed of 500 rpm.

one of the earliest metals used as an electrocatalyst for organic reduction alongside Ni[50,51] and has been studied for the ECH of various substrates.[9,52−54] Furthermore, the activity of the roughened Ag and Zn metals toward deoxygenation of xylose is also notable, which invites the exploration of these catalysts for the valorization of monosaccharides.

3.3. Reaction Pathways for Glucose and Xylose ECH. The reaction pathways for the conversion of glucose and xylose are illustrated in Scheme S1. As ECH reactions were carried out under HER conditions, the hydroxide ions formed from water electrolysis (eq 1) and HER (eq 3) provide alkalinity in the vicinity of the catalyst surface. Under basic conditions, there is increased mutarotation of sugars involving their linear, electroactive form.[55] Consequently, glucose and xylose can isomerize into fructose and xylulose via the Lobry de Bruyn−Van Ekenstein mechanism involving an endiol intermediate. This would result in an increase in the concentration of the ketose isomer of the sugars on the surface of the catalyst as well as in the bulk solution. Direct hydrogenation of glucose yields sorbitol, while hydrogenation of fructose would produce both sorbitol and mannitol (Scheme S1a) as observed on the rough Cu catalyst. Hydrogenation of the endiol form of glucose would also yield both sorbitol and mannitol. The same hydrogenation mechanism would apply to xylose ECH which produces xylitol from xylose and both xylitol and arabitol from xylulose. Experimental results showed that xylitol was formed over all of the studied metal catalysts, while arabitol was formed only on Ag, Cu, and Zn. Considering that fructose and xylulose are the precursors to mannitol and arabitol, respectively, the reactivity of these ketoses toward ECH therefore also depends on the property of the metal catalyst. Based on LSV results for Ag, Au, and Cu, which suggest that ECH occurs concurrently with HER, the mechanism for sugar hydrogenation would involve the addition of chemisorbed hydrogen to the adsorbed substrate. However, for the Zn catalyst, LSV experiments showed that the HER was more facile than either glucose or xylose ECH. Therefore, direct electroreduction of sugars via the PCET mechanism could be the plausible route. To probe this, we carried out ECH tests using rough Zn catalyst at a potential (−0.69 V) with no observable HER (Table S6). Small amounts of sorbitol (0.59 mM) and xylitol (5.43 mM) were observed, which confirms that direct proton and electron transfer mechanisms are possible for the reduction of sugars at least for the rough Zn catalyst.

Further hydrodeoxygenation of the formed sugar alcohols would produce the deoxy sugar products. Significant amounts of 2-deoxylitol were observed from the ECH of xylose on Ag and Zn. However, 2-deoxysorbitol was not detected on any of the catalysts during glucose ECH. The sequential hydrogenation and hydrodeoxygenation reactions are proposed for the formation of 2-deoxylitol starting from xylose (and possibly for 2-deoxysorbitol from glucose) as seen from Scheme S1. The same reaction pathway would apply for the ketose substrates (xylulose and fructose), which leads to the same deoxygenated products. However, the alternative reaction pathway, which involves hydrodeoxygenation as the first step followed by hydrogenation, cannot be ruled out. This would involve an initial hydrodeoxygenation of glucose or xylose to form 2-deoxy-D-glucose and 2-deoxy-D-xylose, respectively, and subsequent hydrogenation of the carbonyl group to form the deoxy sugar products.

Based on the experimental results, the reactivity of sugars toward ECH and the selectivity to different reaction products depend primarily on the chemical nature of the metal catalyst. The presence of hydroxide ions is essential to increase the rate of mutarotation of sugars and make them electroactive. However, too much alkalinity gives rise to undesired side products. On the other hand, operating under HER conditions is necessary to provide chemisorbed hydrogen that is active toward hydrogenation, which then depends mainly on the applied potential. Therefore, the applied potential and pH of the reaction solution must be controlled to optimize the sugar ECH rate and product selectivity.

3.4. Effect of Reaction Parameters on Sugar ECH over Rough Cu. As high activity and selectivity toward sorbitol and xylitol formation were observed with the rough Cu catalysts, ECH reactions were studied further on this catalyst to observe the effects of pH and applied potential on sugar conversion and FE. Electrolysis experiments using the Cu catalyst were carried out in a single-compartment electrochemical cell with pH control as described in Section 2.5. This electrochemical setup allows us to maintain the pH of the bulk solution during electrolysis while keeping the necessary alkalinity within the vicinity of the electrode surface due to the accompanying HER. The pH of the reaction solution can also be controlled using

https://doi.org/10.1021/acscatal.3c04043
ACS Catal. 2023, 13, 14300−14313

buffer solution (e.g., borate buffer); however, it was only suitable for short-term electrolysis where the HER-induced alkalinity can be neutralized within the buffer capacity. Analysis of the products from the single-compartment ECH setup did not show sugar oxidation products as the counter electrode (activated carbon) did not contain metal and the reaction conditions (moderate temperature, pH) were not favorable for sugar electro-oxidation.

Xylose ECH was initially studied at three different pH conditions (pH 5, 7, and 9) with a constant applied potential of −1.0 V. As shown in Figure S20, the highest FE was recorded at pH 9 (24.2%) followed by pH 7 (20.9%) and pH 5 (15.9%). The positive effect of higher pH was also observed in glucose ECH wherein higher conversion was achieved at more alkaline pH.[31] This illustrates the significance of surface alkalinity in promoting the reactivity of sugars. However, a significant amount of xylulose was formed at pH 9 (0.03 mM) from the isomerization of xylose, while negligible amounts of xylulose were observed at pH 5 and 7 (Figure S20). Furthermore, arabitol formation was observed only at pH 7 and pH 9, which would indicate that higher selectivity toward xylitol formation could be achieved at lower pH.

Since appreciable FE was achieved at pH 7 with negligible formation of ketose side products, constant-potential electrolysis experiments were preferentially done at this pH level. Glucose or xylose ECH was carried out at applied potentials of −0.4, −0.7, and −1.0 V (vs RHE). The electrolysis data are presented in Table S7, and FEs toward the hydrogenation products are illustrated in Figure 6. As earlier observed during catalyst screening, the FE toward ECH was higher for xylose than for glucose. For glucose ECH (Figure 6a), higher FE for sorbitol was observed at −0.7 V (2.2%) than at −1.0 V (1.4%), indicating slightly higher reaction selectivity toward the HER at −1.0 V. Similar FEs for mannitol formation was observed at −0.7 V (0.64%) and −1.0 V (0.61%). The lowest glucose ECH activity was observed at −0.4 V due to the lower extent of HER. On the other hand, for xylose ECH (Figure 6b), the FE for xylitol formation increased as the applied potential became more negative and was highest at −1.0 V (21.3%). This suggests that xylose ECH becomes more efficient with more negative applied potentials, possibly due to the greater availability of the linear (electroactive) form of the xylose substrate from the increased level of mutarotation of the sugar (Scheme S1b). The FE for arabitol formation somewhat decreased going from −0.4 V (1.8%) to −1.0 V (1.1%), which may indicate higher selectivity toward xylitol production than arabitol at more negative applied potentials. Compared to previous studies, higher sorbitol FE was obtained using Raney Ni catalyst (57%, pH 3−6),[28] and poor HER catalysts such as Zn (21%, pH = 7)[20] and Pb(Hg) (15%, pH = 7)[20] for the ECH of glucose in a batch configuration. For xylose ECH, Jokic et al. reported a high xylitol FE (>80%, pH 8−8.5) using a Zn(Hg) catalyst.[56] Using a carbon nanotube (CNT)-supported catalysts, Fei et al.[57] obtained sorbitol FEs of 58% (pH = 11) on Zn and 57% (pH = 11) on ZnFe alloy. In our previous work on sugar ECH over mesoporous carbon-supported Au nanocatalysts,[30] a sorbitol FE of 1.2% was obtained for a sorbitol yield of 2.5%, while a xylitol FE of 1.2% was achieved for a xylitol yield of 1.3%.

The significant differences in product yields and FEs between glucose and xylose ECH indicate a difference in reactivity between glucose and xylose under identical reaction conditions by using the same roughened Cu catalyst. This was also observed during the metal screening on all of the metal catalysts studied. A difference in ECH reactivity between glucose and xylose was also observed in our earlier study,[30] wherein a steady increase in FE toward sorbitol production was observed as the applied potentials became more negative, while the opposite trend was observed for xylitol FE. The difference in reactivity was observed to be related to the extent of HER in the presence of glucose or xylose in solution, as studied using *in situ* FTIR-ATR spectroscopy. These suggest a difference in kinetics between glucose and xylose ECH, which also varies with the catalyst being used.

Considering the overall ECH data, the optimum conditions for ECH of these sugars over a Cu catalyst would involve sufficiently negative applied potentials to promote water electrolysis (and, thereby, ECH) and neutral or slightly acidic pH conditions to prevent the formation of ketose side products. The present data provide bases for developing more efficient reaction systems for glucose and xylose ECH. A natural step forward would be to employ supported Cu nanocatalysts to increase the catalyst surface area and, therefore, provide more active sites for sugar ECH.

4. CONCLUSIONS

The ECH of glucose and xylose was studied on electrochemically roughened Ag, Au, Cu, Pt, and Zn metal catalysts. Characterization of the roughened metals showed that electrochemical estimates of surface roughness were consistent with values obtained from physical measurements (i.e., confocal white light microscopy). Besides sorbitol, mannitol was produced over the rough Cu metal presumably from the hydrogenation of fructose. Similarly, arabitol was formed alongside xylitol over Ag, Cu, and Zn, possibly from xylulose as precursor. Aside from hydrogenation products, significant amounts of 2-deoxyxylitol were also observed during xylose ECH over the rough Ag and Zn catalysts. The results obtained illustrate the dependence of the rate of sugar ECH on the property of the metal catalyst, as well as the selectivity toward hydrogenation or deoxygenation products. Furthermore, the yields for the hydrogenation products were higher for xylose ECH than those for glucose in all of the studied catalysts. This may be related to the difference in the extent of HER in the presence of these sugars, as previously observed in our earlier study involving mesoporous carbon-supported Au nanocatalysts.

As the overall rates of glucose and xylose ECH were highest over rough Cu, the effects of different reaction conditions were studied using this catalyst. Higher pH was observed to promote ECH, but excess alkalinity led to the formation of side products. ECH in slightly acidic pH increased the selectivity toward xylitol production, however, at the expense of current efficiency. Therefore, maintaining the reaction solution at a neutral pH would provide appreciable FE while minimizing side reactions. In terms of the applied potential, the FE for xylitol production increased with more negative applied potentials and was highest at −1.0 V (21.3%), while the highest FE for sorbitol formation (2.2%) was observed at a less negative potential (−0.7 V). This illustrates that while a higher potential is required to increase the amount of chemisorbed hydrogen available for ECH, the rate of ECH would also depend largely on the reactivity of the substrate molecule. The results presented in this study provide valuable insights into improving catalytic systems for ECH of sugars by identifying selective catalysts and suitable reaction conditions.

https://doi.org/10.1021/acscatal.3c04043
ACS Catal. 2023, 13, 14300−14313

■ ASSOCIATED CONTENT

Supporting Information

The Supporting Information is available free of charge at https://pubs.acs.org/doi/10.1021/acscatal.3c04043.

Physicochemical characterization of the metal electrodes; determination of ECSA of the roughened metals; Tafel plots for HER; current density vs time profiles during glucose and xylose ECH; ^{1}H NMR spectra and HPLC chromatograms of reaction products from sugar ECH; product selectivity at different time periods during sugar ECH; carbon balance from reaction products; xylose conversion and selectivity between rough and smooth catalysts; comparison of activity and selectivity between Ag catalysts with different geometries; ECSA-normalized yields for sorbitol and xylitol over the rough metal catalysts; estimates of roughness for the metal catalysts before and after ECH tests; SEM images of spent catalysts; reaction schemes for glucose and xylose ECH; ECH data for rough Zn at lower applied potential; Faradaic efficiency (FE) of xylose ECH at different pH conditions; and product yields and FEs of glucose and xylose ECH at different applied potentials (PDF)

■ AUTHOR INFORMATION

Corresponding Author

Henrik Grénman − *Laboratory of Molecular Science and Engineering, Faculty of Science and Engineering, Åbo Akademi University, FI-20500 Turku/Åbo, Finland;* orcid.org/0000-0002-0129-0949; Email: Henrik.Grenman@abo.fi

Authors

Jay Pee Oña − *Laboratory of Molecular Science and Engineering, Faculty of Science and Engineering, Åbo Akademi University, FI-20500 Turku/Åbo, Finland;* orcid.org/0000-0003-2553-0772

Rose Marie Latonen − *Laboratory of Molecular Science and Engineering, Faculty of Science and Engineering, Åbo Akademi University, FI-20500 Turku/Åbo, Finland;* orcid.org/0000-0002-8378-0991

Narendra Kumar − *Laboratory of Molecular Science and Engineering, Faculty of Science and Engineering, Åbo Akademi University, FI-20500 Turku/Åbo, Finland*

Jan-Erik Eriksson − *Laboratory of Molecular Science and Engineering, Faculty of Science and Engineering, Åbo Akademi University, FI-20500 Turku/Åbo, Finland*

Ilari Angervo − *Wihuri Physical Laboratory, Department of Physics and Astronomy, University of Turku, FI-20014 Turku, Finland*

Complete contact information is available at: https://pubs.acs.org/10.1021/acscatal.3c04043

Notes

The authors declare no competing financial interest.

■ ACKNOWLEDGMENTS

This research is part of the FosToBioH2 (From fossil to biohydrogen in Finnish (bio)industry—utilizing electrocatalysis in Aqueous Phase Reforming of hemicelluloses) project conducted at Åbo Akademi University, Finland. The authors gratefully acknowledge the Tiina and Antti Herlin Foundation (Finland) for their financial support. They thank the Wihuri Physical Laboratory, Department of Physics and Astronomy, University of Turku, for the XRD analysis; R. Lassfolk (Turku Center for Chemical and Molecular Analytics, Åbo Akademi) for the NMR Spectroscopy; and L. Silvander (Laboratory Services, Åbo Akademi University) for the SEM analysis.

■ REFERENCES

(1) Akhade, S. A.; Singh, N.; Gutierrez, O. Y.; Lopez-Ruiz, J.; Wang, H.; Holladay, J. D.; Liu, Y.; Karkamkar, A.; Weber, R. S.; Padmaperuma, A. B.; Lee, M. S.; Whyatt, G. A.; Elliott, M.; Holladay, J. E.; Male, J. L.; Lercher, J. A.; Rousseau, R.; Glezakou, V. A. Electrocatalytic Hydrogenation of Biomass-Derived Organics: A Review. *Chem. Rev.* **2020**, *120*, 11370.

(2) Amouzegar, K.; Savadogo, O. Electrocatalytic Hydrogenation of Phenol on Dispersed Pt: Reaction Mechanism and Support Effect. *Electrochim. Acta* **1998**, *43* (5−6), 503.

(3) Amouzegar, K.; Savadogo, O. Electrocatalytic Hydrogenation of Phenol on Dispersed Pt: Effect of Metal Electrochemically Active Surface Area and Electrode Material. *J. Appl. Electrochem.* **1997**, *27* (5), 539.

(4) Amouzegar, K.; Savadogo, O. Electrocatalytic Hydrogenation of Phenol on Highly Dispersed Pt Electrodes. *Electrochim. Acta* **1994**, *39* (4), 557.

(5) Sanyal, U.; Koh, K.; Meyer, L. C.; Karkamkar, A.; Gutiérrez, O. Y. Simultaneous Electrocatalytic Hydrogenation of Aldehydes and Phenol over Carbon-Supported Metals. *J. Appl. Electrochem.* **2021**, *51* (1), 27.

(6) Lopez-Ruiz, J. A.; Sanyal, U.; Egbert, J.; Gutiérrez, O. Y.; Holladay, J. Kinetic Investigation of the Sustainable Electrocatalytic Hydrogenation of Benzaldehyde on Pd/C: Effect of Electrolyte Composition and Half-Cell Potentials. *ACS Sustainable Chem. Eng.* **2018**, *6* (12), 16073.

(7) Sanyal, U.; Lopez-Ruiz, J.; Padmaperuma, A. B.; Holladay, J.; Gutiérrez, O. Y. Electrocatalytic Hydrogenation of Oxygenated Compounds in Aqueous Phase. *Org. Process Res. Dev.* **2018**, *22* (12), 1590.

(8) Song, Y.; Sanyal, U.; Pangotra, D.; Holladay, J. D.; Camaioni, D. M.; Gutiérrez, O. Y.; Lercher, J. A. Hydrogenation of Benzaldehyde via Electrocatalysis and Thermal Catalysis on Carbon-Supported Metals. *J. Catal.* **2018**, *359*, 68.

(9) Lopez-Ruiz, J. A.; Andrews, E.; Akhade, S. A.; Lee, M. S.; Koh, K.; Sanyal, U.; Yuk, S. F.; Karkamkar, A. J.; Derewinski, M. A.; Holladay, J.; Glezakou, V. A.; Rousseau, R.; Gutiérrez, O. Y.; Holladay, J. D. Understanding the Role of Metal and Molecular Structure on the Electrocatalytic Hydrogenation of Oxygenated Organic Compounds. *ACS Catal.* **2019**, *9* (11), 9964.

(10) Qiu, Y.; Xin, L.; Chadderdon, D. J.; Qi, J.; Liang, C.; Li, W. Integrated Electrocatalytic Processing of Levulinic Acid and Formic Acid to Produce Biofuel Intermediate Valeric Acid. *Green Chem.* **2014**, *16* (3), 1305.

(11) Xin, L.; Zhang, Z.; Qi, J.; Chadderdon, D. J.; Qiu, Y.; Warsko, K. M.; Li, W. Electricity Storage in Biofuels: Selective Electrocatalytic Reduction of Levulinic Acid to Valeric Acid or γ-Valerolactone. *ChemSusChem* **2013**, *6* (4), 674.

(12) Matthiesen, J. E.; Suástegui, M.; Wu, Y.; Viswanathan, M.; Qu, Y.; Cao, M.; Rodriguez-Quiroz, N.; Okerlund, A.; Kraus, G.; Raman, D. R.; Shao, Z.; Tessonnier, J. P. Electrochemical Conversion of Biologically Produced Muconic Acid: Key Considerations for Scale-Up and Corresponding Technoeconomic Analysis. *ACS Sustainable Chem. Eng.* **2016**, *4* (12), 7098.

(13) Matthiesen, J. E.; Carraher, J. M.; Vasiliu, M.; Dixon, D. A.; Tessonnier, J. P. Electrochemical Conversion of Muconic Acid to Biobased Diacid Monomers. *ACS Sustainable Chem. Eng.* **2016**, *4* (6), 3575.

(14) Dalavoy, T. S.; Jackson, J. E.; Swain, G. M.; Miller, D. J.; Li, J.; Lipkowski, J. Mild Electrocatalytic Hydrogenation of Lactic Acid to Lactaldehyde and Propylene Glycol. *J. Catal.* **2007**, *246* (1), 15.

(15) Zhao, B.; Chen, M.; Guo, Q.; Fu, Y. Electrocatalytic Hydrogenation of Furfural to Furfuryl Alcohol Using Platinum Supported on Activated Carbon Fibers. *Electrochim. Acta* **2014**, *135*, 139.
(16) Roylance, J. J.; Kim, T. W.; Choi, K. S. Efficient and Selective Electrochemical and Photoelectrochemical Reduction of 5-Hydroxymethylfurfural to 2,5-Bis(Hydroxymethyl)Furan Using Water as the Hydrogen Source. *ACS Catal.* **2016**, *6* (3), 1840.
(17) Kwon, Y.; de Jong, E.; Raoufmoghaddam, S.; Koper, M. T. M. Electrocatalytic Hydrogenation of 5-Hydroxymethylfurfural in the Absence and Presence of Glucose. *ChemSusChem* **2013**, *6* (9), 1659.
(18) Kwon, Y.; Birdja, Y. Y.; Raoufmoghaddam, S.; Koper, M. T. M. Electrocatalytic Hydrogenation of 5-Hydroxymethylfurfural in Acidic Solution. *ChemSusChem* **2015**, *8* (10), 1745.
(19) Kwon, Y.; Koper, M. T. M. Electrocatalytic Hydrogenation and Deoxygenation of Glucose on Solid Metal Electrodes. *ChemSusChem* **2013**, *6* (3), 455.
(20) bin Kassim, A.; Rice, C. L.; Kuhn, A. T. Formation of Sorbitol by Cathodic Reduction of Glucose. *J. Appl. Electrochem.* **1981**, *11* (2), 261.
(21) Anantharaman, V.; Pintauro, P. N. The Electrocatalytic Hydrogenation of Glucose: I. Kinetics of Hydrogen Evolution and Glucose Hydrogenation on Raney Nickel Powder. *J. Electrochem. Soc.* **1994**, *141* (10), 2729.
(22) Park, K.; Pintauro, P. N.; Baizer, M. M.; Nobe, K. Current Efficiencies and Regeneration of Poisoned Raney Nickel in the Electrohydrogenation of Glucose to Sorbitol. *J. Appl. Electrochem.* **1986**, *16* (6), 941.
(23) Pintauro, P. N.; Johnson, D. K.; Park, K.; Baizer, M. M.; Nobe, K. The Paired Electrochemical Synthesis of Sorbitol and Gluconic Acid in Undivided Flow Cells. I. *J. Appl. Electrochem.* **1984**, *14* (2), 209.
(24) Park, K.; Pintauro, P. N.; Baizer, M. M.; Nobe, K. Flow Reactor Studies of the Paired Electro-Oxidation and Electroreduction of Glucose. *J. Electrochem. Soc.* **1985**, *132* (8), 1850.
(25) Liang, Z.; Villalba, M. A.; Marcandalli, G.; Ojha, K.; Shih, A. J.; Koper, M. T. M. Electrochemical Reduction of the Simplest Monosaccharides: Dihydroxyacetone and Glyceraldehyde. *ACS Catal.* **2020**, *10* (23), 13895.
(26) Meyer, L. C.; Sanyal, U.; Stoerzinger, K. A.; Koh, K.; Fulton, J. L.; Camaioni, D. M.; Gutiérrez, O. Y.; Lercher, J. A. Influence of the Molecular Structure on the Electrocatalytic Hydrogenation of Carbonyl Groups and H2Evolution on Pd. *ACS Catal.* **2022**, *12* (19), 11910.
(27) Sauter, W.; Bergmann, O. L.; Schröder, U. Hydroxyacetone: A Glycerol-Based Platform for Electrocatalytic Hydrogenation and Hydrodeoxygenation Processes. *ChemSusChem* **2017**, *10* (15), 3105.
(28) Lessard, J.; Belot, G.; Couture, Y.; Desjardins, S.; Roy, C. The Use of Hydrogen Generated at the Electrode Surface for Electrohydrogenation of Organic Compounds. *Int. J. Hydrogen Energy* **1993**, *18* (8), 681.
(29) Owobi-Andely, Y.; Fiaty, K.; Laurent, P.; Bardot, C. Use of Electrocatalytic Membrane Reactor for Synthesis of Sorbitol. *Catal. Today* **2000**, *56* (1−3), 173.
(30) Oña, J. P.; Latonen, R.-M.; Kumar, N.; Peurla, M.; Angervo, I.; Grénman, H. Electrocatalytic Hydrogenation and Oxidation of Glucose and Xylose on Mesoporous Carbon-Supported Au Nanocatalysts. *Electrochim. Acta* **2023**, *437*, 141536.
(31) Oña, J. P.; Latonen, R.-M.; Kumar, N.; Peurla, M.; Angervo, I.; Grénman, H. Electrocatalytic Hydrogenation of Glucose and Xylose Using Carbon Fiber Supported Au Nanocatalysts. *Electrochim. Acta* **2022**, *426*, 140754.
(32) Cave, E. R.; Shi, C.; Kuhl, K. P.; Hatsukade, T.; Abram, D. N.; Hahn, C.; Chan, K.; Jaramillo, T. F. Trends in the Catalytic Activity of Hydrogen Evolution during CO2 Electroreduction on Transition Metals. *ACS Catal.* **2018**, *8* (4), 3035.
(33) Andérez Fernández, M.; Rissanen, J.; Pérez Nebreda, A.; Xu, C.; Willför, S.; García Serna, J.; Salmi, T.; Grénman, H. Hemicelluloses from Stone Pine, Holm Oak, and Norway Spruce with Subcritical Water Extraction—Comparative Study with Characterization and Kinetics. *J. Supercrit. Fluids* **2018**, *133*, 647.
(34) Yedro, F. M.; Grénman, H.; Rissanen, Jv.; Salmi, T.; García-Serna, J.; Cocero, M. J. Chemical Composition and Extraction Kinetics of Holm Oak (Quercus Ilex) Hemicelluloses Using Subcritical Water. *J. Supercrit. Fluids* **2017**, *129*, 56.
(35) Gallina, G.; Cabeza, Á.; Grénman, H.; Biasi, P.; García-Serna, J.; Salmi, T. Hemicellulose Extraction by Hot Pressurized Water Pretreatment at 160 °C for 10 Different Woods: Yield and Molecular Weight. *J. Supercrit. Fluids* **2018**, *133*, 716−725, DOI: 10.1016/j.supflu.2017.10.001.
(36) Nebreda, A. P.; Grénman, H.; Mäki-Arvela, P.; Eränen, K.; Hemming, J.; Willför, S.; Murzin, D. Y.; Salmi, T. Acid Hydrolysis of O-Acetyl-Galactoglucomannan in a Continuous Tube Reactor: A New Approach to Sugar Monomer Production. *Holzforschung* **2016**, *70* (3), 187.
(37) Lu, X.; Junghans, P.; Wärnå, J.; Hilpmann, G.; Lange, R.; Trajano, H.; Eränen, K.; Estel, L.; Leveneur, S.; Grénman, H. Hydrolysis of Semi-Industrial Aqueous Extracted Xylan from Birch (Betula Pendula) Employing Commercial Catalysts: Kinetics and Modelling. *J. Chem. Technol. Biotechnol.* **2022**, *97* (1), 130.
(38) Lu, X.; Junghans, P.; Weckesser, S.; Wärnå, J.; Hilpmann, G.; Lange, R.; Trajano, H.; Eränen, K.; Estel, L.; Leveneur, S.; Grénman, H. One Flow through Hydrolysis and Hydrogenation of Semi-Industrial Xylan from Birch (Betula Pendula) in a Continuous Reactor-Kinetics and Modelling. *Chem. Eng. Process.* **2021**, *169*, 108614.
(39) Lian, W.; Wang, L.; Song, Y.; Yuan, H.; Zhao, S.; Li, P.; Chen, L. A Hydrogen Peroxide Sensor Based on Electrochemically Roughened Silver Electrodes. *Electrochim. Acta* **2009**, *54* (18), 4334.
(40) Mie, Y.; Takayama, H.; Hirano, Y. Facile Control of Surface Crystallographic Orientation of Anodized Nanoporous Gold Catalyst and Its Application for Highly Efficient Hydrogen Evolution Reaction. *J. Catal.* **2020**, *389*, 476.
(41) Chen, C. S.; Handoko, A. D.; Wan, J. H.; Ma, L.; Ren, D.; Yeo, B. S. Stable and Selective Electrochemical Reduction of Carbon Dioxide to Ethylene on Copper Mesocrystals. *Catal. Sci. Technol.* **2015**, *5* (1), 161.
(42) Weremfo, A.; Fong, S. T. C.; Khan, A.; Hibbert, D. B.; Zhao, C. Electrochemically Roughened Nanoporous Platinum Electrodes for Non-Enzymatic Glucose Sensors. *Electrochim. Acta* **2017**, *231*, 20.
(43) Gu, R. A.; Shen, X. Y.; Liu, G. K.; Ren, B.; Tian, Z. Q. Surface-Enhanced Raman Scattering from Bare Zn Electrode. *J. Phys. Chem. B* **2004**, *108*, 17519.
(44) McCrory, C. C. L.; Jung, S.; Peters, J. C.; Jaramillo, T. F. Benchmarking Heterogeneous Electrocatalysts for the Oxygen Evolution Reaction. *J. Am. Chem. Soc.* **2013**, *135* (45), 16977.
(45) Schmidt, S. A.; Kumar, N.; Zhang, B.; Eränen, K.; Murzin, D. Y.; Salmi, T. Preparation and Characterization of Alumina-Based Microreactors for Application in Methyl Chloride Synthesis. *Ind. Eng. Chem. Res.* **2012**, *51* (12), 4545.
(46) Wang, S.; Lu, A.; Zhong, C. J. Hydrogen Production from Water Electrolysis: Role of Catalysts. *Nano Convergence*. **20218**. DOI: 10.1186/s40580-021-00254-x.
(47) Sarac, B.; Karazehir, T.; Mühlbacher, M.; Sarac, A. S.; Eckert, J. Electrocatalytic Behavior of Hydrogenated Pd-Metallic Glass Nanofilms: Butler-Volmer, Tafel, and Impedance Analyses. *Electrocatalysis* **2020**, *11* (1), 94.
(48) Bao, F.; Kemppainen, E.; Dorbandt, I.; Bors, R.; Xi, F.; Schlatmann, R.; van de Krol, R.; Calnan, S. Understanding the Hydrogen Evolution Reaction Kinetics of Electrodeposited Nickel-Molybdenum in Acidic, Near-Neutral, and Alkaline Conditions. *ChemElectroChem* **2021**, *8* (1), 195.
(49) Schouten, K. J. P.; Kwon, Y.; Van Der Ham, C. J. M.; Qin, Z.; Koper, M. T. M. A New Mechanism for the Selectivity to C1 and C2 Species in the Electrochemical Reduction of Carbon Dioxide on Copper Electrodes. *Chem. Sci.* **2011**, *2* (10), 1902.
(50) Belot, G.; Desjardins, S.; Lessard, J. Electrocatalytic Hydrogenation of Organic Compounds on Devarda Copper and Raney

Nickel Electrodes in Basic Media. *Tetrahedron Lett.* **1984**, *25* (47), 5347.
(51) Yamada, T.; Osa, T.; Matsue, T. Hydrogenation of Benzene Ring by Paired Electrosynthesis with Raney-Nickel Cathode. *Chem. Lett.* **1987**, *16* (10), 1989.
(52) Andrews, E.; Lopez-Ruiz, J. A.; Egbert, J. D.; Koh, K.; Sanyal, U.; Song, M.; Li, D.; Karkamkar, A. J.; Derewinski, M. A.; Holladay, J.; Gutiérrez, O. Y.; Holladay, J. D. Performance of Base and Noble Metals for Electrocatalytic Hydrogenation of Bio-Oil-Derived Oxygenated Compounds. *ACS Sustainable Chem. Eng.* **2020**, *8* (11), 4407.
(53) Dabo, P.; Mahdavi, B.; Ménard, H.; Lessard, J. Selective Electrocatalytic Hydrogenation of 2-Cyclohexen-1-One to Cyclohexanone. *Electrochim. Acta* **1997**, *42* (9), 1457.
(54) Ivanova, N. M.; Soboleva, E. A.; Kulakova, E.; Malyshev, V. P.; Kirilyus, Iv. Reduction of Nitrophenols in an Electrocatalytic System. *Russ. J. Appl. Chem.* **2009**, *82* (3), 421.
(55) Isbell, H. S.; Pigman, W. Mutarotation of Sugars in Solution : PART II. Catalytic Processes, Isotope Effects, Reaction Mechanisms, and Biochemical Aspects. *Adv. Carbohydr. Chem. Biochem.* **1969**, *24*, 13.
(56) Jokic, A.; Ristic, N.; Jaksic, M. M.; Spasojevic, M.; Krstajic, N. Simultaneous Electrolytic Production of Xylitol and Xylonic Acid from Xylose. *J. Appl. Electrochem.* **1991**, *21* (4), 321.
(57) Fei, S.; Chen, J.; Yao, S.; Deng, G.; Nie, L.; Kuang, Y. Electroreduction of α-Glucose on CNT/Graphite Electrode Modified by Zn and Zn-Fe Alloy. *J. Solid State Electrochem.* **2005**, *9* (7), 498.

https://doi.org/10.1021/acscatal.3c04043
ACS Catal. 2023, 13, 14300−14313